Capillarity

Vol. 3, No. 4, p. 62-74, 2020

Invited review

Applications of mercury intrusion capillary pressure for pore structures: A review

Liang Jiao[1], Pål Østebø Andersen[2], Junping Zhou[3], Jianchao Cai[1,4]*

[1]*Institute of Geophysics and Geomatics, China University of Geosciences, Wuhan 430074, P. R. China*

[2]*Department of Energy Resources, University of Stavanger, Kjell Arholms Gate 41, 4036 Stavanger, Norway*

[3]*State Key Laboratory of Coal Mine Disaster Dynamics and Control, Chongqing University, Chongqing 400044, P. R. China*

[4]*State Key Laboratory of Petroleum Resources and Prospecting, China University of Petroleum, Beijing 102249, P. R. China*

Keywords:
Capillary pressure
mercury intrusion capillary pressure
pore structure
fractal
permeability

Cited as:
Jiao, L., Andersen, P.Ø., Zhou, J., Cai, J. Applications of mercury intrusion capillary pressure for pore structures: A review. *Capillarity*, 2020, 3(4): 62-74, doi: 10.46690/capi.2020.04.02.

Abstract:
The shape, size, and connectivity of porous structures control the overall storage capacity and flow in oil and gas reservoirs. The mercury intrusion capillary pressure (MICP) technique is widely utilized to measure capillary pressure and calculate pore size distribution of core samples in the geo-energy industry. Combining the MICP capillary pressure data with parameters from other experimental methods (such as scanning electron microscopy, and nuclear magnetic resonance) or theoretical approaches (such as fractal theory) can more accurately describe the pore structure of reservoirs. In this paper, the latest advances on the application of primary drainage MICP curves from reservoir porous structures are reviewed in three main aspects: The measurement and calculation of MICP capillary pressure, estimation of pore size distributions making use of fractal characteristics, and determination of permeability. Experimental measurements and numerical simulation methods of MICP capillary pressure with its influencing factors are also discussed. MICP capillary pressure combined with other methods are argued to be one of the main directions for future research on reservoir pore structures.

1. Introduction

Capillary pressure, the pressure difference between two immiscible fluids forming interfaces in porous media, is an essential physical parameter to study the pore structure and the fluid flow in rocks (Li et al., 2020a). Capillary pressure is caused by the interaction force of internal fluids and boundary solid (Vavra, 1992). It not only controls the static distribution of reservoir fluids before production but also the distribution of residual oil and gas after production (Dakhelpour-Ghoveifel et al., 2019). Above all, mercury intrusion capillary pressure (MICP) can provide indirect information of pore structure and effective permeability in porous media (He and Hua, 1998; Tian et al., 2012; Liu et al., 2016; Huang et al., 2018).

One of the most important application of MICP is quantifying the pore structure and theoretically evaluating the quality of oil/gas reservoirs (Purcell, 1949; Tiab and Donaldson, 2004; Dakhelpour-Ghoveifel et al., 2019). The pores act as storage sites and migration paths for fluids in porous media (e.g., oil and gas), so fluid flow is influenced by microscopic pore characteristics (Tsakiroglou and Payatakes, 2000; Tian et al., 2012; Liu et al., 2016). However, it is difficult to describe its microscopic characteristics accurately due to the complexity and irregularities in porous media (Wang et al., 2012; Cai et al., 2016).

In the geo-energy industry, accurate capillary pressure is required to interpret the porous medium properties (Chung and Lin, 2017; Dejam, 2018). Experimental capillary pressure curves can be measured by MICP, centrifuge, high pressure semipermeable membrane, etc (Li et al., 2020a). Among them, MICP is a useful and economical technique in oil and natural gas development (Semnani et al., 2019). However, it relies on the use of mercury which is a strongly non-wetting phase and this may not reflect true reservoir conditions. The main advantage is that the method is strongly sensitive to the pore throat size distribution as the incremental injection of mercury must overcome increasing threshold pressures as smaller pores are invaded. MICP is typically used for studying micro-pore structures and pore size distributions (PSD) of reservoir rocks (Purcell, 1949; Cerepi et al., 2002; Torabi et al., 2013; Liu and Ostadhassan, 2019). However, a great deal of studies

Yandy Scientific Press

*Corresponding author.
E-mail address: jliang5052@foxmail.com (L. Jiao); pal.andersen@uis.no (P.Ø. Andersen); zhoujp1982@sina.com (J. Zhou); caicj@cug.edu.cn (J. Cai).

Received November 15, 2020; revised November 28, 2020; accepted November 29, 2020; available online December 2, 2020.

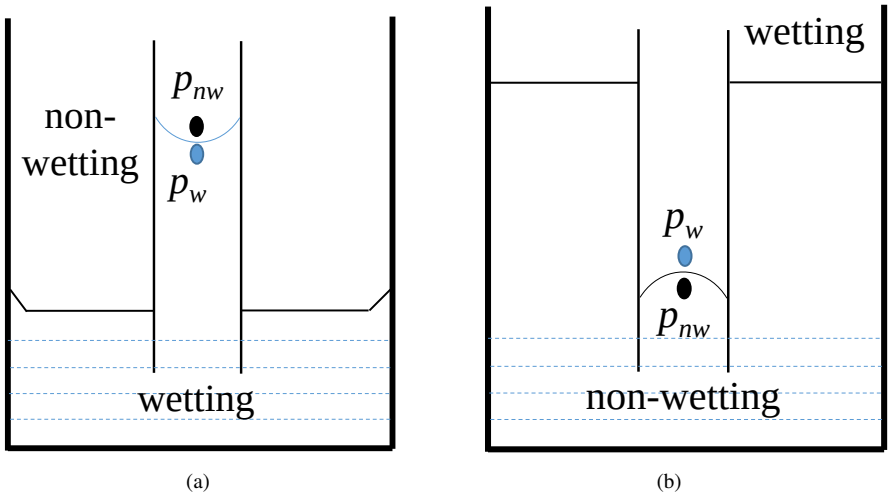

Fig. 1. Capillary pressure in capillaries. (a) The capillary bundle is put into the wetting phase; (b) The capillary bundle is put into the non-wetting phase.

have shown that very high mercury intrusion pressures may damage the pore structure of rock samples because such high pressure is larger than the pressure at which reservoir rocks can be compressed, especially for softer shale and siltstones (Zhu et al., 2010; Yang et al., 2014; Peng et al., 2017; Huang et al., 2019). While MICP can quantify the pore space and hence porosity, a limitation is that it cannot determine irreducible wetting saturation (Li et al., 2020a). Researchers have found that the pore structure characteristics of reservoirs can be accurately analyzed by combining MICP with experimental methods (such as X-ray computer tomography (X-CT) (Arns et al., 2005; Knackstedt et al., 2007), scanning electron microscopy (SEM) (Zhao et al., 2020), and nuclear magnetic resonance (NMR) (Cheng et al., 2019) or theoretical approaches (such as fractal theory) (Mandelbrot, 1982; Krohn, 1988; He and Hua, 1998). Fractal geometry gave a new method for describing complex and irregular structures (Mandelbrot, 1982). The macro-heterogeneity and micro-pore structures of the pore space have been proven to have fractal characteristics (Mandelbrot, 1982; Krohn, 1988; He and Hua, 1998; Xie et al., 2010; Lai and Wang, 2015; Hao et al., 2017), so it is a preferred method to describe the pore structure characteristics of reservoirs using fractal dimension calculated from MICP curves data (Friesen and Mikula, 1987; Angulo et al., 1992; Shen and Li, 1994; Li, 2010; Yang et al., 2016; Su et al., 2018; Li et al., 2019; Guo et al., 2020).

The connectivity and the PSD are closely related to the permeability of porous media (Purcell, 1949; Allen, 1974; Giesche, 2010; Nooruddin et al., 2014). MICP can be combined with fractal theory to study the pore structure, which provides information on the effective permeability (He and Hua, 1998; Li, 2010a). In some unconventional reservoirs permeability measurement cannot be carried out directly (Gueguen et al., 1995; Comisky et al., 2007; Nooruddin et al., 2014). Hence, accurate permeability estimation using available MICP data is a good alternative. Theoretical models (based on bundle-of-tubes assumptions) and empirical models to estimate permeability from MICP include the Purcell model (Purcell, 1949), Winland model (Kolodzie Jr, 1980), Swanson model (Swanson, 1981), and Pittman model (Pittman, 1992), however effective predictions is still challenging.

Herein, we explain the theory of capillary pressure in porous media, and analyze the latest application and improvement of MICP. Then, we summarize the application of MICP on characterizing pore structure and predicting permeability with some emphasis on how fractal characteristics are used. A discussion of limitations and future directions for MICP in reservoir pore structures are proposed.

2. Background of capillary pressure

The non-wetting and wetting phase fluids create a pressure difference over their interface to move the periphery of the meniscus towards the wetting phase, exemplified by a capillary tube in Fig. 1 (Butt et al., 2003; Moghadam et al., 2020). The capillary pressure p_c is defined as the pressure difference, $p_c = p_{nw} - p_w$, between non-wetting phase pressure p_{nw} and wetting phase pressure p_w. In actual reservoirs, the impact of a pore size distribution leads the two-phase domain to become a transition zone extending a certain height (Fig. 2).

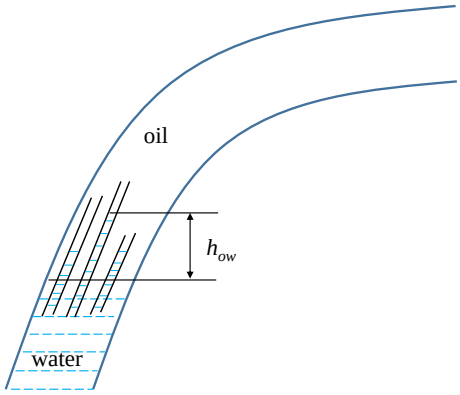

Fig. 2. Diagram of oil-water transition zone (how is the oil-water transition zone).

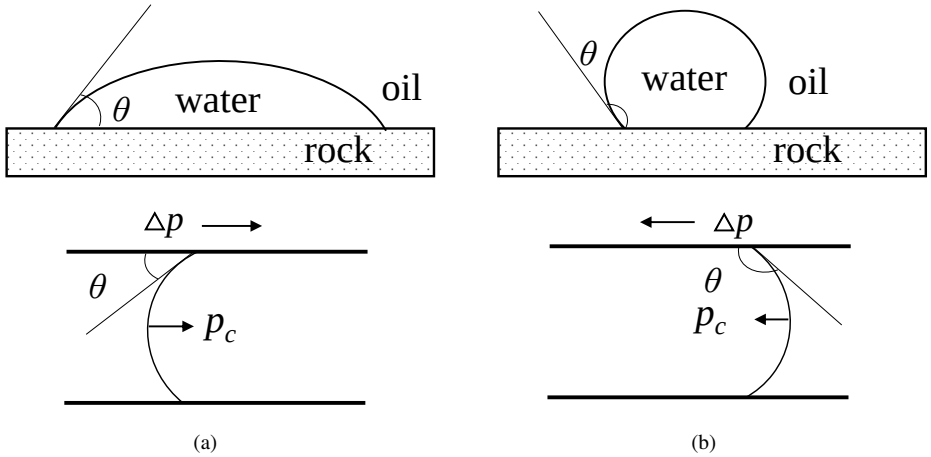

Fig. 3. Diagram of water flooding under different wettability conditions.

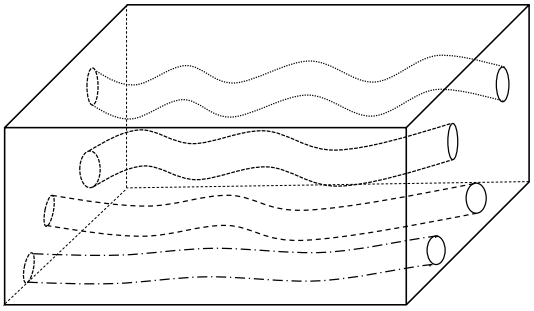

Fig. 4. Diagram of capillary tube model.

A pore surface displacement process is shown in Fig. 3 (Vavra, 1992). Fig. 3(a) shows that if the pore surface is water-wet, water automatically enters the core under the action of capillary pressure to displace oil. More generally, the wetting fluid displaces the non-wetting fluid on the surface. Fig. 3(b) shows that the pore surface of the rock is oil-wetted. In this case, same as in Fig. 1(b), the capillary pressure causes resistance to water displacing oil and the rock surface cannot automatically absorb water. Therefore, an external force must be applied to overcome the capillary pressure.

3. Experimental measurement of the MICP

The benefit of the MICP test is that it provides continuous information on porous structures and pore throat distributions (Comisky et al., 2011). Mercury is injected into a rock sample, as a strongly non-wetting fluid. In the analysis of MICP tests, the porous media is commonly assumed composed of capillary bundles with unequal diameters as shown in Fig. 4 (Sigal, 2013; Wang et al., 2018b). When the injection pressure is higher than the capillary threshold pressure corresponding to the pore throat, the pores are invaded by mercury. Therefore, the injection pressure is equivalent to the capillary pressure and the capillary radius is the pore radius. MICP experiments have been reported to apply maximum mercury intrusion capillary pressure up to approximate 276 MPa, which makes mercury theoretically enters minimum pore radius as small as 2.7 nm (Wang et al., 2018b).The mathematical relationship between capillary pressure and pore radius is connected by Young-Laplace equation (Eq. (1)).

$$p_c = \frac{2\sigma\cos\theta}{r} \tag{1}$$

where p_c is the mercury intrusion capillary pressure, σ is the surface tension, θ is the contact angle between the mercury and the rock, r is the pore radius.

After the pressure injection reaches a defined maximum value, it can be lowered to let the mercury saturation reduce. This mercury ejection is an imbibition process, as shown later in Fig. 6(a) and typically results in different curves compared to the mercury injection capillary pressure curves.

According to the Young-Laplace equation, the maximum pore radius corresponds to the minimum capillary pressure/displacement pressure p_{cd}, $p_{cd} = 2\sigma\cos\theta/r_{max}$, which is the capillary pressure of the largest connecting pore throat in pore system when the non-wetting phase fluid begins to enter core pores. This is the capillary pressure that must be overcome before mercury will enter the sample. p_{cd} is one of the main parameters to evaluate storage and seepage and is closely related to permeability. Reservoirs with good permeability have low p_{cd}. Fig. 5 shows the relationship between displacement pressure p_{cd} and different pore structure parameters in low permeability sandstones (Wang et al., 2018a). Fig. 5(a) indicates that p_{cd} decreases in power-law with increasing sorting coefficient. Greater sorting coefficient means that the PSD range is wide. The pore space then has access to large pores with good connectivity. Fig. 5(b) shows that p_{cd} decreases by power-law as median pore radius R_{50} increases. Fig. 5(c) shows p_{cd} decreases with porosity. Fig. 5(d) shows p_{cd} has a strong and negative correlation with tortuosity. With displacement pressure p_{cd} increasing, sorting coefficient, median pore radius R_{50}, and porosity decrease and tortuosity increases, indicating PSD and pore structures become more complex.

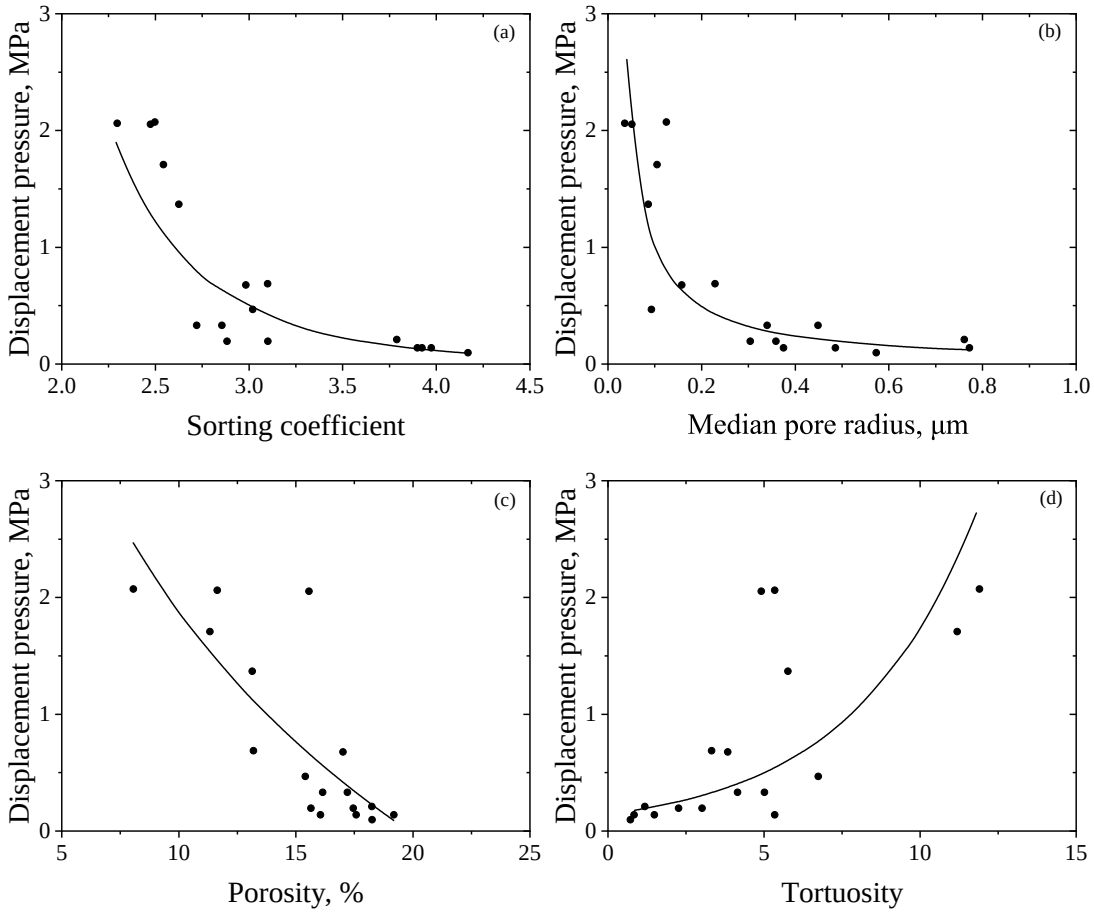

Fig. 5. The relationship between displacement pressure pcd and pore structure parameters (from Wang et al., 2018a).

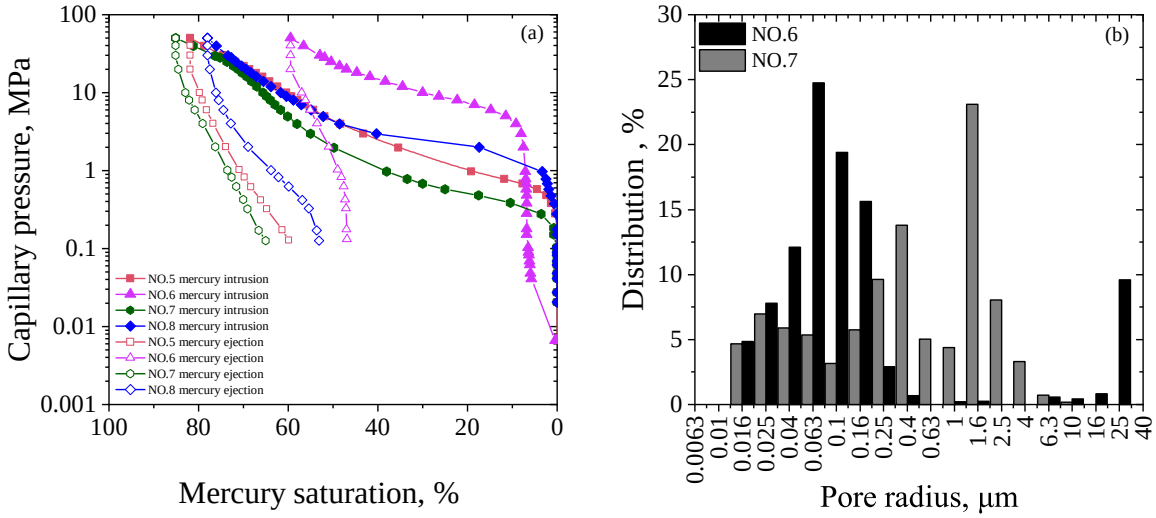

Fig. 6. (a) capillary pressure curves (NO. 5 porosity: 15.7%, permeability, 1.04 mD. NO. 6 porosity: 5.3%, permeability, 0.04 mD. NO. 7 porosity: 14.1%, permeability, 2.2 mD. NO. 8 porosity: 11.1%, permeability, 0.36 mD) and (b) pore size distribution.

3.1 Application of capillary pressure curve

The MICP capillary pressure curve is a viable measure for characterizing the pore structure, which is controlled by the sorting and size of the pore-throats. As shown in Fig. 6(a), the middle flat segment of NO. 7 curve is longer than others in sandstone samples indicating that pore distribution represented in the middle flat segment is more uniform. The middle flat segment is closer to the horizontal axis indicating the larger the major pore radius in the rock samples. Fig. 6(b) shows the pore size distributions from MICP calculation of core samples No.6 and No. 7. The pore size varies from several nanometers to dozens of micrometers. The maximum pore radius distribution is largest between 1 and 1.6 μm of core NO. 7 and is located between 0.063 and 0.1 nm of core NO. 6. These phenomena can explain the reason why porosity (14.1%) and permeability (2.2 mD) of NO.7 physical parameters are largely outweigh those (5.3% and 0.04 mD) of NO.6. Meaningfully, it is reasonable to analyze the pore structure characteristics through the capillary pressure curve, further studying the relevant parameters of PSD and percolation ability.

Several studies (Purcell, 1949; Olson and Grigg, 2008; Comisky et al., 2011) show the usefulness of MICP for determining porosity of small or irregular rock samples. Combining capillary pressure curves with petrophysical properties in porous media, capillary pressure data can be employed to obtain numerous related parameters (specific surface area, permeability contribution, J function curve, average pore radius, maximum pore radius, sorting coefficient, displacement pressure, relative permeability, PSD, wettability, etc.) of reservoir properties. Considering the above capillary pressure parameters, the pore structure can be effectively evaluated.

3.2 Improvement of experimental measurement

As for unconventional reservoirs, the traditional MICP experimental results may produce some errors caused by different types of pores (micro fractures, vugs, etc.), wettability, Jamin effect. Therefore, scholars have proposed different improvement measures to enhance its applicability. Li et al. (2020a) conducted a self-developed capillary pressure measurement method (SDM) to measure the in-situ capillary pressure under reservoir condition (SDM-R) for low permeability rock in the laboratory. SDM can determine directly capillary pressure caused by the difference between the water and oil pressures in primary drainage case. The capillary pressure obtained by MICP need to be converted. The same core samples were segmented into two parts (the porosity and permeability are the same) to conduct SDM and MICP, respectively. Fig. 7 (the physical parameters are shown in Table 1) shows that the capillary pressures through the conversion of MICP method are slightly higher than in-situ capillary pressures because of the former higher relative error in converted capillary pressure. Sun et al. (2020) found a reciprocating MICP technique as shown in Fig. 8, which presents the increment of mercury intrusion the original sample and repeated mercury injection into the same sample. It can be observed that the increase of

Table 1. The physical property parameters corresponding to the rock sample in Figure 7 (from Li et al., 2020a).

Core NO.	Porosity, %	Air permeability, mD
1	7.6	0.173
2	9.2	0.394
3	11.5	0.614

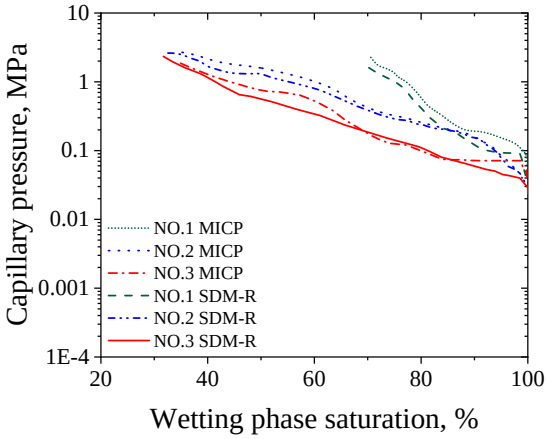

Fig. 7. Comparison between capillary pressures obtained from different measurement methods (from Li et al., 2020a).

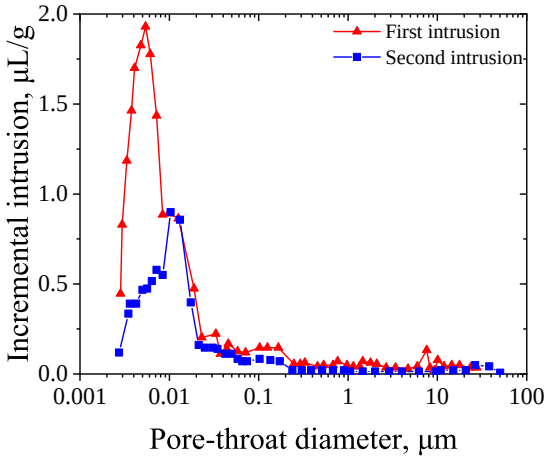

Fig. 8. Pore-throat diameters of original and re-intrusion samples (from Sun et al., 2020).

the second mercury intrusion is lower than the initial mercury injection, and the results proved that the high pressure may not generate new micro-fractures and damage shale samples pore structure. Although reciprocating MICP is secondary drainage method, the influence of the residual saturation formed at the first mercury intrusion on the results is ignored.

Jia et al. (2019) found that capillary pressure decreased by changing the wettability of coal samples from water-wet to strong gas-wet to improve fluid microscopic flow characteristics, thus coalbed methane recovery was significantly enhanced. Hussien et al. (2019) proposed methods to reduce

Table 2. Capillary pressure models in literature.

References	Model	Comments
Corey (1954)	$\frac{1}{p_c^2} = CS_w^*$	$S_w^* = \frac{S_w - S_{wc}}{1 - S_{wc} - S_{nwr}}$, C is a constant, S_w is the wetting phase saturation, S_{wc} is the minimum wetting phase saturation, S_{nwr} is the residual non-wetting phase saturation
Thomeer (1960)	$p_c = p_e \left(\frac{S_{Hg}}{S_{Hg\infty}} \right)^{-\frac{1}{F_g}}$	S_{Hg} is the mercury saturation, $S_{Hg\infty}$ is the mercury saturation with maximum capillary pressure, p_e is the entry capillary pressure, and F_g is the pore shape factor (dimensionless)
Brooks-Corey (1964)	$p_c = p_e (S_w^*)^{-\frac{1}{\lambda}}$	λ is pore size distribution index
Van Genuchten (1980)	$S_w^* = [1 + (\alpha p_c)^n]^{-m}$	α, n, and m are independent parameters, $S_w^* = \frac{S_w - S_{wc}}{1 - S_{wc}}$
Jing and Van Wunnik (1998)	$p_c = p_c^0 \left[\left(\frac{d}{S_w - S_{wc}} \right)^{n_0} + a \right]$	a, d, and n_0 are parameters, which have to be obtained according to actual conditions, p_c^0 is scaling factor of the capillary pressure
Oostrom and Lenhard (1998)	$S_w^* = [1 + (\alpha_0 \beta p_c)^{n_1}]^{-m_0}$	α_0, n_1, and m_0 are independent parameters, β is interfacial tension
Li and Horne (2001)	$p_c = p_{\max} (1 - S_w^*)^{-\frac{1}{\lambda}}$	p_{max} is the maximum capillary pressure
Li (2010a)	$p_c = p_{\max} (1 - bS_w^*)^{-\frac{1}{\lambda_0}}$	$b = 1 - \left(\frac{p_e}{p_{\max}} \right)^{-\lambda_0}$, $\lambda_0 = 3 - D_f$, D_f is the fractal dimension
Kim et al. (2011)	$S_w = 1 - (1 - S_{wc}) \exp \left(\frac{-F_g}{\log(p_{cd}/p_e)} \right)$ (drainage-type) $S_w = S_{wc} + (1 - S_{nwr}) \exp \left(\frac{-F_g}{\log(p_{ci}/-p_e)} \right)$ (imbibition-type)	p_{ci} is the imbibition capillary pressure
Wang et al. (2019b)	$p_c = [p_{\max}^{-\lambda} - (p_{\max}^{-\lambda} - p_e^{-\lambda}) S_w]^{-\frac{1}{\lambda_1}}$	$\lambda_1 = 3 - D_T - D_f$, D_T is the tortuosity fractal dimension

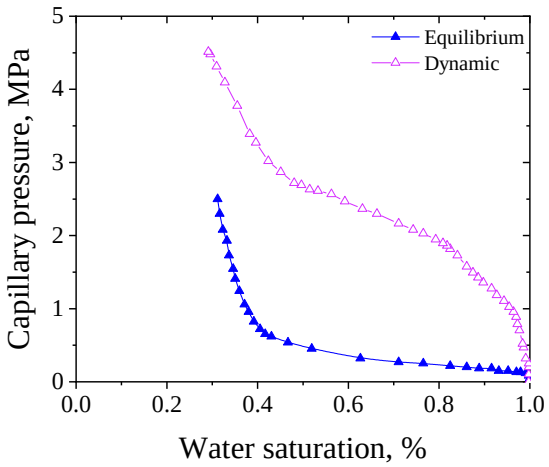

Fig. 9. Dynamic and static capillary pressure (from Li et al., 2017).

the contact angle by using surfactant, and increased the temperature and pressure, thereby reducing the capillary pressure and promoting the desorption of gas to achieve the purpose of increasing shale gas production. Simultaneously, contact angle can influence capillary pressure, and capillary pressure decreases with the increasing contact angle (Culligan et al., 2004). Li et al. (2019) studied the effect of fractures on dynamic capillary pressure of rock samples because of the contact angle improvement in fractured media.

Additionally, the capillary pressure under the equilibrium state of wetting phase and non-wetting phase interface is conventionally measured (Tian et al., 2012; Li et al., 2020b). In such a state, capillary pressure is expressed as the function of fluid saturation, which is invariable with time. However, multiphase flow is regarded to be dynamic (Li et al., 2020b). Fig. 9 shows capillary pressure curves present two characteristics: the dynamic capillary pressure, and the static capillary pressure under equilibrium condition to characterize the multiphase flow (Li et al., 2017). The dynamic capillary pressure is larger than the static capillary pressure in lowest permeability, and the difference is obvious the reason why the increase of two immiscible fluids interfaces curvature generates a higher capillary pressure in dynamic conditions than that in static conditions (Mirzaei and Das, 2007; Zhao et al., 2008; Li et al., 2017).

3.3 Numerical models based on experimental measurement

Many studies have proposed empirical or theoretical capillary pressure models as seen in Table 2 where important reservoir parameters are included in the expressions. Brooks and Corey (1964) proposed a capillary pressure model (B-C

model) relationship between normalized wetting phase saturation and capillary pressure. However, The B-C model does not properly match MICP curves of microfracture rocks. Li and Horne (2006) coupled the B-C model with fractal modeling, and got close match to experimental MICP capillary pressure data from the Geysers rocks with a considerable amount of microfractures. Subsequently, Li (2010a) found a more general capillary pressure model from fractal geometry to analyze the rock in which the Brooks-Corey model can match and the rock in which the Brooks-Corey model cannot match. Interestingly, the quantitative determination the heterogeneity and complexity of different rock samples used fractal dimension is consistent with the conventional qualitative method considering the frequency diagram of PSD based on the previous theoretical basis. Wang et al. (2019b) expressed a new capillary pressure model introducing both the fractal dimension and tortuosity fractal dimension which is the fractal distribution of tortuosity describing streamtubes tortuous or meandering. Meanwhile, Kim et al. (2011) analyzed different types (drainage-type and imbibition-type) capillary pressure models in carbonate rock including macropores and micropores.

4. Capillary pressure and fractal characteristics for pore structure

Many researches showed that the reservoir pore space presents fractal characteristics, and the fractal theory has been considerably used for characterizing the microscopic pore structure (Zhu et al., 2011; Cai et al., 2015; Ji et al., 2016). Based on MICP experiment, it is also a new method to study the pore structure of reservoirs (Yu et al., 2019).

4.1 Fractal models

Mandelbrot first proposed the fractal theory, which is used to characterize and evaluate the pore structure characteristics (Mandelbrot, 1982).

$$N(r) \propto r^{-D_f} \tag{2}$$

where $N(r)$ is the number of capillary tubes with radius r, D_f is the fractal dimension, a measure of the complexity and irregularity of porous media, which is a key physical parameter to analyze the distribution and heterogeneity of pore structures in reservoir rocks. Capillary pressure and fluid saturation present a power-law function relationship, its index is related to the fractal dimension of the rock pore surface (Brooks and Corey, 1964; Angulo et al., 1992). Considerable studies showed that it is reasonable by matching the general fractal model to experimental MICP data to obtain the fractal dimension (Angulo et al., 1992; Shen and Li, 1994; Li, 2010a). The number of capillary tubes $N(r)$ is derived from the mercury intrusion experiment data. Li (2010b) expressed the $N(r)$ as given by

$$N(r) = \frac{V_{Hg}}{\pi r^2 l} \tag{3}$$

where V_{Hg} is the cumulative volume of mercury intrusion when the measured pore radius is r, l is the core length.

Substituting Eq. (3) into Eq. (2),

$$\frac{V_{Hg}}{\pi r^2 l} \propto r^{-D_f} \tag{4}$$

l is a constant, arranging Eq. (4),

$$V_{Hg} \propto r^{2-D_f} \tag{5}$$

As pore radius r can be represented by mercury intrusion capillary pressure p_c based on Eq. (1), and V_{Hg} can be represented by mercury saturation S_{Hg}.

Eq. (5) can be expressed as:

$$S_{Hg} \propto p_c^{(D_f-2)} \tag{6}$$

Differentiating Eq. (6),

$$\frac{dS_{Hg}}{dp_c} \propto p_c^{(D_f-3)} \tag{7}$$

Friesen and Mikula (1987) proposed a three-dimensional geometric fractal model in a different case that a three-dimensional pore model ($N(r) = V_{Hg}/\pi r^3$) instead of a two-dimensional capillary tube model. The fractal model can then be expressed as:

$$\frac{dS_{Hg}}{dp_c} \propto p_c^{(D_f-4)} \tag{8}$$

He and Hua (1998) proposed a different theoretical model for calculating the fractal dimension. The authors assumed that pore volume is defined as αr^3, where α is a constant related to pore shape, and neglected the minimum pore radius ($r_{min} \ll r_{max}$). Considering the relationship between the displacement pressure, capillary pressure, and wetting phase fluid saturation, the calculation formula can be expressed as follows

$$S_w \propto \left(\frac{p_c}{p_{cd}}\right)^{(D_f-3)} \tag{9}$$

where S_w is wetting phase saturation, p_{cd} is the displacement pressure. Hao et al. (2017) calculated the fractal dimension of the sandstone rock samples of the Yanchang Formation in the Ordos Basin using Eq. (9). Eq. (9) presents the relationship between saturation of the wetting phase and capillary pressure. However, the wetting phase saturation cannot measure directly from MICP method due to the higher adhesive forces between the wetting phase and the rock surface (Zhang et al., 2016).

Furthermore, the thermodynamic analysis during the MICP experiment, a new thermodynamic model (Eq. (10)) for calculating the fractal dimension is shown (Zhang and Li, 1995; Zhang et al., 2006). The theoretical fractal dimension can be used to determine the roughness and heterogeneity of the surface of the porous medium.

$$\ln\left(\frac{W_n}{r_n^2}\right) = D_f \ln\left(\frac{V_n^{1/3}}{r_n}\right) + C \tag{10}$$

where W_n is the cumulative surface energy during the mercury intrusion process, $W_n = \sum_{i=1}^{n} p_{ci} V_i$, p_{ci} and V_i are the MICP and

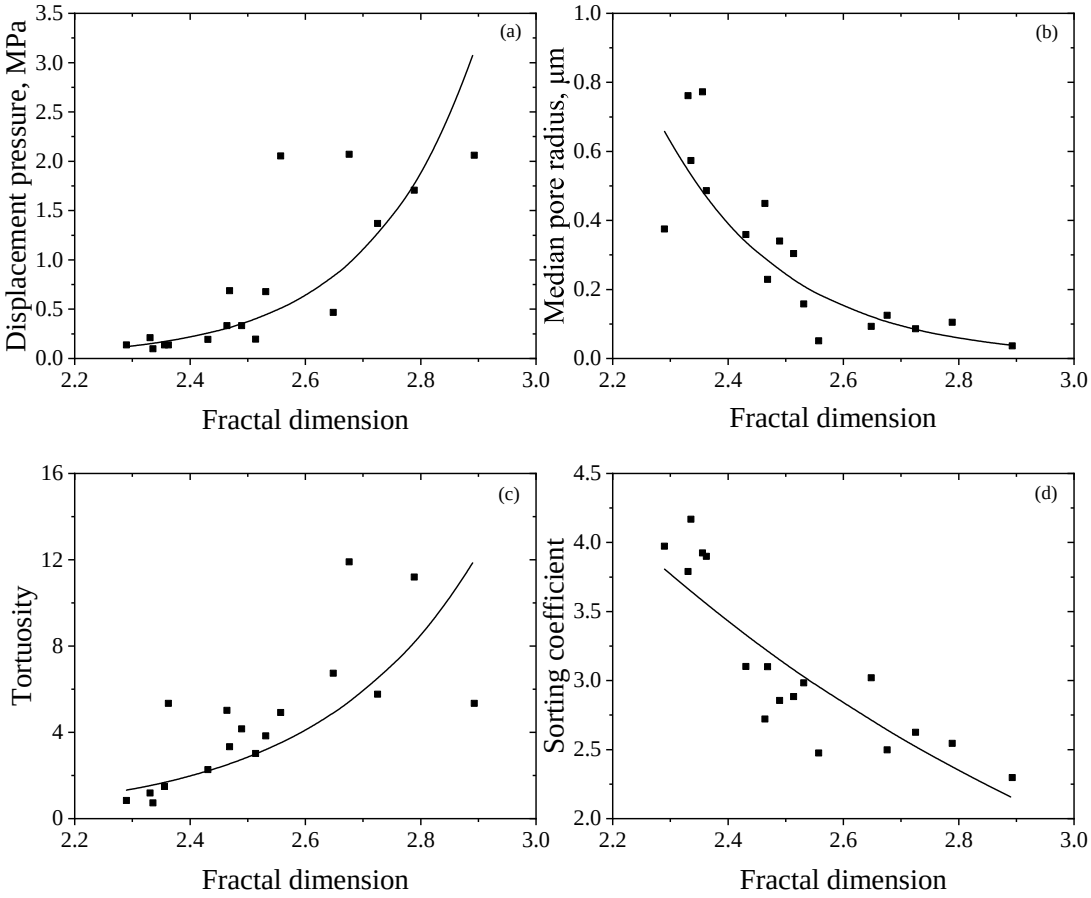

Fig. 10. The correlation between the fractal dimensions and pore structure parameters (from Wang et al., 2018a).

increased mercury volume at stage i, respectively, V_n is the intrusion volume of mercury, and r_n is pore radius.

Using the capillary pressure curve data of the drainage case in Fig. 6, different mathematical models have been developed to calculate the fractal dimension (Li, 2010b; Su et al., 2018). Based on the fractal theory, studies showed that the micropores, transitional pores, and mesopores fractal dimensions were evaluated theoretically using the high-pressure mercury intrusion (HPMI) experiment data (Li et al., 2017). The HPMI experiment systems can inject mercury pressures up to 400 MPa (Moghadam et al., 2020). The heterogeneity of pore structure in Chang 7 low-permeability sandstone reservoirs were studied by values of fractal dimension, and the larger fractal dimension means that pore structures are irregular and heterogeneous in porous medium (Li et al., 2017; Guo et al., 2020). This may explain the universal applicability and effectiveness of the model.

4.2 Fractal characteristic analysis

Considering the different fractal models, Wang et al. (2018a, 2018b) used the capillary pressure data obtained from conventional MICP and HPMI experiments to calculate the fractal dimension. The authors studied the pore structure characteristics of low-permeability sandstone and carbonate rock samples respectively. Fig. 10 shows that the relationship between the fractal dimensions (in three-dimensional space) and pore structure parameters of carbonate rock samples. As the fractal dimension increases, the displacement pressure and tortuosity increase exponentially, the corresponding pores and channels become smaller and more tortuous. The sorting coefficient and median radius decrease continuously with the fractal dimension increases. Consequently, as fractal dimension increases, the pore structure is getting more complex.

In the above models, only the fractal dimension of the pore space was considered, and the effect of pore geometric tortuosity is neglected. Considering the tortuosity of pores, a new model for calculating the fractal dimension was derived (Su et al., 2018) . The model is expressed as:

$$\log S_{Hg} \propto (D_f + D_T - 3) \log p_c \tag{11}$$

where D_T is the tortuosity fractal dimension.

Although various models can be used to calculate the fractal dimension using MICP curves data in the section 4, it failed to indicate which fractal dimension is the most suitable for characterizing the reservoir pore structure.

5. Calculated Permeability with MICP data

Permeability is one of the important petrophysical properties of the reservoir (Pape et al., 1999). MICP capillary pressure can be used to estimate it.

Theoretical models and analysis

The porosity and pore radius corresponding to the mercury saturation during the MICP process were used as independent variables to establish the empirical permeability equation. Eq. (12) is the classical Winland model (Kolodzie Jr, 1980).

$$\log r_{35} = 0.732 + 0.588 \log K - 0.864 \log \phi \tag{12}$$

where r_{35} is the pore radius with 35% mercury saturation, K is the permeability, ϕ is the porosity.

Wang et al. (2018a) used the Winland model to predict the permeability of low permeability sandstone reservoirs based on capillary pressure data, and found optimal permeability prediction equation corresponding to pore size r_5 as a constraint for low permeability sandstones.

$$\log r_5 = 0.4664 \log K + 0.6831 \log \phi + 2.1297 \tag{13}$$

where r_5 is the pore radius with 5% mercury saturation. There are many factors that affect permeability. Zhang et al. (2017) found that the permeability of tight sandstone reservoirs has a poor correlation with porosity, and proposed two models (Eqs. (14) and (15)) to predict permeability.

$$\log d_{\max} = 1.899 + 1.712 \log K + 0.844 \log \phi \tag{14}$$

$$\log d_f = 0.948 + 1.263 \log K + 0.838 \log \phi \tag{15}$$

where $d_{\max}$ is pore diameter with displacement pressure, d_f is the pore diameter at inflection point, which is the boundary of different pore types (intergranular and intercrystalline pores) indicting that the seepage capability of porous media worsens.

In order to accurately predict the permeability of low-permeability sandstone reservoirs, Guo et al. (2020) proposed a new model Eq. (16) of permeability prediction considering fractal dimension.

$$\log K = -2.027 + \frac{2.555}{D_f} - \frac{0.033}{r_n} \tag{16}$$

where r_n is the pore size corresponding to capillary pressure.

Permeability is controlled by pore throat sizes, which is closely related to displacement pressure p_{cd} mentioned in section 4 (Schmitt et al., 2015; Lai et al., 2018). Purcell (1949) illustrated that the square of reciprocal of capillary pressure corresponds to permeability change. In fractal porous media, capillary pressure and fractal method can be used to model fluid flow (Buiting and Clerke, 2013; Cai et al., 2017). Yu and Cheng (2002) proposed a fractal permeability model for calculating the permeability, considering capillary diameter distribution and tortuous capillary tubes conform to fractal characteristic in porous media, respectively. The prediction model is expressed as:

$$K = \frac{\pi}{128} \frac{L_0^{1-D_T}}{A} \frac{D_f}{3 + D_T - D_f} \lambda_{\max}^{3+D_T} \tag{17}$$

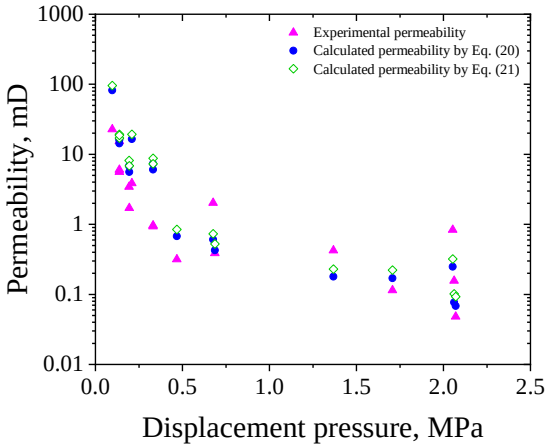

Fig. 11. The correlation between the permeability and p_{cd} (from Wang et al., 2018a).

where $\lambda_{\max}$ is the maximum pore diameter, as $\lambda_{\max}$ can be expressed with mercury saturation p_{cd}, substituting Eq. (1) into Eq. (17),

$$K = \frac{\pi (4\sigma \cos\theta)^{3+D_T}}{128} \frac{L_0^{1-D_T}}{A} \frac{D_f}{3 + D_T - D_f} p_{cd}^{-(3+D_T)} \tag{18}$$

where L_0 is the representative length, A is the area of cross section and $A = L_0^2$. Wang et al. (2019a) took the tortuosity characteristics into account when the fluid flows in a single tortuous capillary tube and then developed a new prediction permeability model.

$$K = \frac{\pi}{32(3 + D_T)} \frac{L_0^{1-D_T}}{A} \frac{D_f}{3 + D_T - D_f} \lambda_{\max}^{3+D_T} \tag{19}$$

Similarly, Eq. (20) can be rewritten as:

$$K = \frac{\pi (4\sigma \cos\theta)^{3+D_T}}{32} \frac{L_0^{1-D_T}}{(D_T + 3)A} \frac{D_f}{3 + D_T - D_f} p_{cd}^{-(3+D_T)} \tag{20}$$

Eq. (20) is similar to Eq. (18). When $D_T = 1$, the improved mathematical models (Eqs. (18) and (20)) can be simplified as:

$$K = 2\pi (\sigma \cos\theta)^4 \frac{D_f}{4 - D_f} p_{cd}^{-4} \tag{21}$$

As fluid flows through the capillary bundle. Fig. 11 presents experimental permeability compared with calculated permeability using different fractal permeability models (Eqs. (20) and (21)). It indicates that the power function relationship between permeability and p_{cd}, and permeability will decrease significantly as capillary pressure increases.

The factors of pore size and porosity are considered in these models, which are applicable to conventional reservoirs. The permeability of Eq. (12) is calculated by porosity. For low-permeability reservoirs with poor correlation between porosity and permeability, the calculated results are more different from the actual measured values. In Eqs. (14) and (15), the threshold values $d_{\max}$ and d_f, important factors affecting permeability, which make the permeability change significantly, were

considered. The porosity in Eq. (16) was replaced by fractal dimension, and it provided a new direction for the permeability prediction. Eqs. (14), (15), and (16) are considerable modified based on Eq. (12).

6. Discussion and future works

Further study of MICP capillary pressure combined with other methods can provide better characterization of reservoir pore structure.

1) Capillary pressure curve can be used to characterize the microstructure characteristics of the reservoir. The widely used MICP method has incompleteness in unconventional reservoirs. In order to accurately investigate the pore structure characteristics of unconventional reservoirs, a combination of MICP curves and other methods, such as X-CT, SEM, and NMR, can be used.
2) Based on the MICP experiment, different fractal models are used to calculate fractal dimensions to characterize the reservoir pore structure, and study the relationship between the fractal dimension and petrophysical properties. However, due to the large differences in reservoirs and different physical parameters, the fractal dimension calculated by fractal models cannot indicate the most applicable model corresponding to specific reservoir. Therefore, how to select the most suitable model needs to be considered in future work.
3) Combining MICP data to predict reservoir permeability, frequent methods are obtained empirically, but the empirical parameters may not be correlate in the same way or be sufficient for each reservoir. Therefore, more factors need to be considered to make the predicted permeability more accurate.

7. Conclusions

Reservoir pore structure characteristics determine the oil and gas reservoirs storage and flow capacity. The MICP experiment is an effective method to infer the pore structure of reservoirs. A combination of parameters from MICP curves are used to estimate permeability and other parameters. This article analyzed the application research of MICP. Based on fractal theory and MICP curve data, the fractal dimension is used to evaluate the pore structure and petrophysical properties of the reservoir.

Acknowledgement

Andersen acknowledges the Research Council of Norway and the industry partners, ConocoPhillips Skandinavia AS, Aker BP ASA, Vår Energi AS, Equinor ASA, Neptune Energy Norge AS, Lundin Norway AS, Halliburton AS, Schlumberger Norge AS, Wintershall DEA, of The National IOR Centre of Norway for support, and Cai acknowledges support from the National Natural Science Foundation of China (No. 41722403).

Conflict of interest

The authors declare no competing interest.

References

Allen, T. Particle Size Measurement. New York, USA, Chapman and Hall, 1974.

Angulo, R.F., Alvarado, V., Gonzalez, H. Fractal dimensions from mercury intrusion capillary tests. Paper SPE 23695 Presented at SPE Latin America Petroleum Engineering Conference, Caracas, Venezuela, 8-11 March, 1992.

Arns, C.H., Bauget, F., Limaye, A., et al. Pore-scale characterization of carbonates using X-ray microtomography. SPE J. 2005, 10(4): 475-484.

Brooks, R., Corey, A. Hydraulic properties of porous media. Hydrol. Pap. 1964, 7: 892-898.

Buiting, J.J.M., Clerke, E.A. Permeability from porosimetry measurements: Derivation for a tortuous and fractal tubular bundle. J. Pet. Sci. Eng. 2013, 108: 267-278.

Butt, H.J., Graf, K., Kappl, M. Physics and Chemistry of Interface. Weinheim, Germany, Wiley-VCH Verlag GmbH & Co. KGaA, 2003.

Cai, J., Luo, L., Ye, R., et al. Recent advances on fractal modeling of permeability for fibrous porous media. Fractals 2015, 23(1): 1540006.

Cai, J., Wei, W., Hu, X., et al. Fractal characterization of dynamic fracture network extension in porous media. Fractals 2017, 25(2): 1750023.

Cai, Y., Liu, D., Pan, Z., et al. Investigating the effects of seepage-pores and fractures on coal permeability by fractal analysis. Transp. Porous Media 2016, 111(2): 479-497.

Cerepi, A., Durand, C., Brosse, E. Pore microgeometry analysis in low-resistivity sandstone reservoirs. J. Pet. Sci. Eng. 2002, 35(3): 205-232.

Cheng, Z., Ning, Z., Yu, X., et al. New insights into spontaneous imbibition in tight oil sandstones with NMR. J. Pet. Sci. Eng. 2019, 179: 455-464.

Chung, C., Lin, H. Enhancing immiscible fluid displacement in porous media by capillary pressure discontinuities. Transp. Porous Media 2017, 120(2): 309-325.

Comisky, J., Newsham, K., Rushing, J., et al. A Comparative study of capillary-pressure-based empirical models for estimating absolute permeability in tight gas sands. Paper SPE 110050 Presented at SPE Annual Technical Conferencend Exhibition, Anaheim, California, 11-14 November, 2007.

Comisky, J.T., Santiago, M., McCollom, B., et al. Sample size effects on the application of mercury injection capillary pressure for determining the storage capacity of tight gas and oil shales. Paper SPE 149432 Presented at SPE Canadian Unconventional Resources Conference, Calgary, Alberta, 15-17 November, 2011.

Corey, A.T. The interrelation between gas and oil relative permeabilities. Prod. Mon. 1954, 19(1): 38-41.

Culligan, K.A., Wildenschild, D., Christensen, B., et al. Interfacial area measurements for unsaturated flow

through a porous medium. Water Resour. Res. 2004, 40(12): 1-12.

Dakhelpour-Ghoveifel, J., Shegeftfard, M., Dejam, M. Capillary-based method for rock typing in transition zone of carbonate reservoirs. J. Pet. Explor. Prod. Technol. 2019, 9(3): 2009-2018.

Dejam, M. The role of fracture capillary pressure on the block-to-block interaction process. J. Porous Media 2018, 21(11): 1121-1136.

Friesen, W.I., Mikula, R.J. Fractal dimensions of coal particles. J. Colloid Interface Sci. 1987, 120(1): 263-271.

Giesche, H. Mercury porosimetry: A general (practical) overview. Part. Part. Syst. Charact. 2010, 23(1): 9-19.

Gueguen, Y., Palciauskas, V., Jeanloz, R. Introduction to the physics of rocks. Phys. Today 1995, 48(4): 87-88.

Guo, R., Xie, Q., Qu, X., et al. Fractal characteristics of pore-throat structure and permeability estimation of tight sandstone reservoirs: A case study of Chang 7 of the upper triassic Yanchang formation in Longdong area, Ordos Basin, China. J. Pet. Sci. Eng. 2020, 184: 106555.

Hao, L., Tang, J., Wang, Q., et al. Fractal characteristics of tight sandstone reservoirs: A case from the upper triassic Yanchang formation, Ordos Basin, China. J. Pet. Sci. Eng. 2017, 158: 243-252.

He, C., Hua, M. Fractal geometry description of reservoir pore structure. Oil and Gas Geology 1998, 19(1): 15-23. (in Chinese)

Huang, H., Chen, L., Dang, W., et al. Discussion on the rising segment of the mercury extrusion curve in the high pressure mercury intrusion experiment on shales. Mar. Pet. Geol. 2019, 102: 615-624.

Huang, S., Wu, Y., Meng, X., et al. Recent advances on microscopic pore characteristics of low permeability sandstone reservoirs. Adv. Geo-Energy Res. 2018, 2(2): 122-134.

Hussien, O.S., Elraies, K.A., Almansour, A., et al. Experimental study on the use of surfactant as a fracking fluid additive for improving shale gas productivity. J. Pet. Sci. Eng. 2019, 183: 106426.

Ji, W., Song, Y., Jiang, Z., et al. Fractal characteristics of nano-pores in the lower silurian Longmaxi shales from the upper Yangtze platform, south China. Mar. Pet. Geol. 2016, 78: 88-98.

Jia, L., Li, K., Zhou, J., et al. Experimental study on enhancing coal-bed methane production by wettability alteration to gas wetness. Fuel 2019, 255: 115860.

Jing, X., Wunnik, J. A capillary pressure function for interpretation of core-scale displacement experiments. Paper SCA 9807 Presented at Centre for Petroleum Studies, Imperial College, UK, 14-22 September, 1998.

Kim, K., Lee, Y., Hwang, S., et al. Improved capillary pressure model considering dual-pore geometry system in carbonate reservoirs. J. Pet. Sci. Eng. 2011, 78(3): 601-608.

Knackstedt, M.A., Sok. R., Adrian. S., et al. 3D pore scale characterisation of carbonate core: Relating pore types and interconnectivity to petrophysical and multiphase flow properties. Paper IPTC 11775 Presented at International Petroleum Technology Conference, Dubai, U.A.E, 4-6 December, 2007.

Kolodzie Jr, S. Analysis of pore throat size and use of the Waxman-Smits equation to determine OOIP in spindle field colorado. Paper SPE 9382 Presented at SPE Annual Technical Conference and Exhibition, Dallas, Texas, 21-24 September, 1980.

Krohn, C.E. Fractal measurements of sandstones, shales, and carbonates. J. Geophys. Res. 1988, 93: 3297-3305.

Lai, J., Wang, G. Fractal analysis of tight gas sandstones using high-pressure mercury intrusion techniques. J. Nat. Gas Sci. Eng. 2015, 24: 185-196.

Lai, J., Wang, G., Wang, Z., et al. A review on pore structure characterization in tight sandstones. Earth-Sci. Rev. 2018, 177: 436-457.

Li, K. More general capillary pressure and relative permeability models from fractal geometry. J. Contam. Hydrol. 2010a, 111 (1): 13-24.

Li, K. Analytical derivation of Brooks-Corey type capillary pressure models using fractal geometry and evaluation of rock heterogeneity. J. Pet. Sci. Eng. 2010b, 73(1-2): 20-26.

Li, K., Horne, R.N. An experimental and analytical study of steam/water capillary pressure. SPE Reserv. Eval. Eng. 2001, 4(6): 477-482.

Li, K., Horne, R.N. Fractal modeling of capillary pressure curves for the Geysers rocks. Geothermics 2006, 35(2): 198-207.

Li, P., Zheng, M., Bi, H., et al. Pore throat structure and fractal characteristics of tight oil sandstone: A case study in the Ordos Basin, China. J. Pet. Sci. Eng. 2017a, 149: 665-674.

Li, Y., Cui, X., Li, H., et al. An in-situ capillary pressure measurement method to characterize pore structure of tight formation. J. Pet. Sci. Eng. 2020a, 192: 107270.

Li, Y., Li, H., Chen, S., et al. Capillarity characters measurement and effects analysis in different permeability formations during waterflooding. Fuel 2017b, 194: 129-143.

Li, Y., Li, H., Chen, S., et al. Investigation of the dynamic capillary pressure during displacement process in fractured tight rocks. AICHE J. 2019, 66(12): e16783.

Li, Y., Luo, H., Li, H., et al. A brief review of dynamic capillarity effect and its characteristics in low permeability and tight reservoirs. J. Pet. Sci. Eng. 2020b, 189: 106959.

Liu, K., Ostadhassan, M. The impact of pore size distribution data presentation format on pore structure interpretation of shales. Adv. Geo-Energy Res. 2019, 3(2): 187-197.

Liu, P., Yuan, Z., Li, K. An improved capillary pressure model using fractal geometry for coal rock. J. Pet. Sci. Eng. 2016, 145: 473-481.

Mandelbrot, B. B. The Fractal Geometry of Nature. New York, USA, W. H. Freeman, 1982.

Mirzaei, M., Das, D.B. Dynamic effects in capillary pressure-saturations relationships for two-phase flow in 3D porous media: Implications of micro-heterogeneities. Chem. Eng. Sci. 2007, 62(7): 1927-1947.

Moghadam, A., Vaisblat, N., Harris, N.B., et al. On the magnitude of capillary pressure (suction potential) in tight rocks. J. Pet. Sci. Eng. 2020, 190: 107133.

Nooruddin, H.A., Hossain, M.E., Al-Yousef, H., et al. Comparison of permeability models using mercury injection capillary pressure data on carbonate rock samples. J. Pet. Sci. Eng. 2014, 121: 9-22.

Olson, R.K., Grigg, M.W. Mercury injection capillary pressure (MICP) a useful tool for improved understanding of porosity and matrix permeability distributions in shale reservoirs. Paper Presented at AAPG Annual Convention, San Antonio, TX, USA, 20-23 April, 2008.

Oostrom, M., Lenhard, R.J. Comparison of relative permeability-saturation-pressure parametric models for infiltration and redistribution of a light nonaqueous-phase liquid in Sandy porous media. Adv. Water Resour. 1998, 21(2): 145-157.

Pape, H., Clauser, C., Iffland, J. Permeability prediction based on fractal pore-space geometry. Geophysics 1999, 64(5): 1447-1460.

Peng, S., Zhang, T., Loucks, R.G., et al. Application of mercury injection capillary pressure to mudrocks: Conformance and compression corrections. Mar. Pet. Geol. 2017, 88: 30-40.

Pittman, E.D. Relationship of porosity and permeability to various parameters derived from mercury injection-capillary pressure curves for sandstone. AAPG Bull. 1992, 76(2): 191-198.

Purcell, W.R. Capillary pressures-their measurement using mercury and the calculation of permeability therefrom. J. Pet. Technol. 1949, 1(2): 39-48.

Schmitt, M., Fernandes, C.P., Wolf, F.G., et al. Characterization of Brazilian tight gas sandstones relating permeability and angstrom-to micron-scale pore structures. J. Nat. Gas Sci. Eng. 2015, 27: 785-807.

Semnani, A.K., Shahverdi, H., Khaz'ali, A.R. Averaging the experimental capillary pressure curves for scaling up to the reservoir condition in the imbibition process. J. Pet. Sci. Eng. 2019, 184: 106539.

Shen, P., Li, K. A new method for determining the fractal dimension of pore structures and its application. Paper Presented at Proceedings of the 10th Offshore South East Asia Conference, Singapore, 6-9 December, 1994.

Sigal, R.F. Mercury capillary pressure measurements on Barnett core. SPE Reserv. Eval. Eng. 2013, 16(4): 432-442.

Su, P., Xia, Z., Qu, L., et al. Fractal characteristics of low-permeability gas sandstones based on a new model for mercury intrusion porosimetry. J. Nat. Gas Sci. Eng. 2018, 60: 246-255.

Sun, M., Zhang, L., Hu, Q., et al. Multiscale connectivity characterization of marine shales in southern China by fluid intrusion, small-angle neutron scattering (SANS), and FIB-SEM. Mar. Pet. Geol. 2020, 112: 104101.

Swanson, B.F. A simple correlation between permeabilities and mercury capillary pressures. J. Pet. Technol. 1981, 33(12): 2498-2504.

Thomeer, J.H.M. Introduction of a pore geometrical factor defined by the capillary pressure curve. J. Pet. Technol. 1960, 12(3): 73-77.

Tiab, D., Donaldson, E.C. Petrophysics: Theory and Practice of Measuring Reservoir Rock and Fluid Transport Properties. Amsterdam, Netherlands, Gulf Professional Pub, 2004.

Tian, S., Lei, G., He, S., et al. Dynamic effect of capillary pressure in low permeability reservoirs. Pet. Explor. Dev. 2012, 39(3): 405-411.

Torabi, A., Fossen, H., Braathen, A. Insight into petrophysical properties of deformed sandstone reservoirs. AAPG Bull. 2013, 97(4): 619-637.

Tsakiroglou, C.D., Payatakes, A.C. Characterization of the pore structure of reservoir rocks with the aid of serial sectioning analysis, mercury porosimetry and network simulation. Adv. Water Resour. 2000, 23(7): 773-789.

Van Genuchten, M.T. A closed-form equation for predicting the hydraulic conductivity of unsaturated soils. Soil Sci. Soc. Am. J. 1980, 44(5): 892-898.

Vavra, C.L. Geological applications of capillary pressure: A review. AAPG Bull. 1992, 76(6): 840-850.

Wang, F., Jiao, L., Lian, P., et al. Apparent gas permeability, intrinsic permeability and liquid permeability of fractal porous media: Carbonate rock study with experiments and mathematical modelling. J. Pet. Sci. Eng. 2019a, 173: 1304-1315.

Wang, F., Jiao, L., Liu, Z., et al. Fractal analysis of pore structures in low permeability sandstones using mercury intrusion porosimetry. J. Porous Media 2018a, 21(11): 1097-1119.

Wang, F., Jiao, L., Zhao, J., et al. A more generalized model for relative permeability prediction in unsaturated fractal porous media. J. Nat. Gas Sci. Eng. 2019b, 67: 82-92.

Wang, F., Lian, P., Jiao, L., et al. Fractal analysis of microscale and nanoscale pore structures in carbonates using high-pressure mercury intrusion. Geofluids 2018b, 2018: 4023150.

Wang, H., Liu, Y., Song, Y., et al. Fractal analysis and its impact factors on pore structure of artificial cores based on the images obtained using magnetic resonance imaging. J. Appl. Geophys. 2012, 86: 70-81.

Xie, S., Cheng, Q., Ling, Q., et al. Fractal and multifractal analysis of carbonate pore-scale digital images of petroleum reservoirs. Mar. Pet. Geol. 2010, 27(2): 476-485.

Yang, M., Meng, Y., Li, G., et al. Effect of grain size and grain content on the hardness and drillability of rocks. Sains Malays. 2014, 43(1): 81-87.

Yang, R., He, S., Yi, J., et al. Nano-scale pore structure and fractal dimension of organic-rich Wufeng-Longmaxi shale from Jiaoshiba area, Sichuan Basin: Investigations using FE-SEM, gas adsorption and helium pycnometry. Mar. Pet. Geol. 2016, 70: 27-45.

Yu, B., Cheng, P. A fractal permeability model for bi-dispersed porous media. Int. J. Heat Mass Transf. 2002, 45(14): 2983-2993.

Yu, Y., Luo, X., Wang, Z., et al. A new correction method for mercury injection capillary pressure (MICP) to characterize the pore structure of shale. J. Nat. Gas Sci. Eng. 2019, 68: 102896.

Zhang, B., Li, S. Determination of the surface fractal dimension for porous media by mercury porosimetry. Ind. Eng. Chem. Res. 1995, 34(4): 1383-1386.

Zhang, B., Liu, W., Liu, X. Scale-dependent nature of the surface fractal dimension for bi- and multi-disperse porous solids by mercury porosimetry. Appl. Surf. Sci. 2006, 253(3): 1349-1355.

Zhang, L., Lu, S., Xiao, D., et al. Pore structure characteristics of tight sandstones in the northern Songliao Basin, China. Mar. Pet. Geol. 2017, 88: 170-180.

Zhang, X., Wu, C., Li, T. Comparison analysis of fractal characteristics for tight sandstones using different calculation methods. J. Geophys. Eng. 2016, 14(1): 120-131.

Zhao, J., Hu, Q., Liu, K., et al. Pore connectivity characterization of shale using integrated wood's metal impregnation, microscopy, tomography, tracer mapping and porosimetry. Fuel 2020, 259: 116248.

Zhao, G., Zhu, J., Guan, L. Method of applying capillary pressure data to calculate initial oil saturation. Journal of China University of Petroleum, China: Edition of Natural Science 2008, 32(4): 38-41. (in Chinese)

Zhu, Q., Xie, M., Yang, J., et al. A fractal model for the coupled heat and mass transfer in porous fibrous media. Int. J. Heat Mass Transf. 2011, 54(7-8): 1400-1409.

Zhu, Y., Chen, S., Fang, J., et al. The geologic background of the Siluric shale-gas reservoiring in Szechwan, China. J. China Coal Soc. 2010, 35: 1160-1164.